




Correlated photon pair propagation in circuit QED with superconducting processors

Sayan Lahiri , Suman Mondal , Kanhaiya Pandey, and Tapan Mishra
Department of Physics, Indian Institute of Technology, Guwahati 781039, India

 (Received 10 March 2020; revised 16 July 2020; accepted 25 September 2020; published 15 October 2020)

We propose a method to achieve photon pair propagation in an array of three-level superconducting circuits. Assuming experimentally accessible three-level artificial atoms with strong anharmonicity coupled via microwave transmission lines in both one and two dimensions we analyze the circuit quantum electrodynamics (QED) of the system. We explicitly show that, for a suitable choice of the coupling ratio between different levels, the single-photon propagation is suppressed and the propagation of photon pairs emerges. This propagation of photon pairs leads to the pair superfluid of polaritons associated with the system. We compute the complete phase diagram of the polariton quantum matter revealing the pair superfluid phase which is sandwiched between the vacuum and the Mott insulator state corresponding to the polariton density equal to 2 in the strong-coupling regime.

DOI: [10.1103/PhysRevA.102.043710](https://doi.org/10.1103/PhysRevA.102.043710)

I. INTRODUCTION

The phenomenon of pairing plays significant roles in different areas of fundamental physics ranging from condensed matter to atomic, molecular, and nuclear physics. Typically, in such systems, the two-body attractions lead to the formation of bound states of constituent particles. However, in some specific cases, the bound pairs can be formed even in the presence of two-particle repulsion, e.g., in Cooper pairs of electrons [1] or in a superconductor. The two-body interactions whether attractive or repulsive lead to the formation of bound states of constituent particles. These pairs, under proper conditions, may have significant contributions in establishing novel and exotic physical phenomena and contribute to technological applications. In recent years the simplest such pair formations (attractive and repulsive) have been predicted and experimentally observed in the context of interacting ultracold atomic systems in optical lattices [2–4]. These observations rely on the sophisticated control over the parameters associated with the optical lattice strength and/or the technique of Feshbach resonance [5]. Although the atomic or molecular systems provide promising platforms to simulate several complex quantum many-body phenomena, there are certain limitations that cannot be avoided due to various reasons. In particular, the formation of attractive pairs will require a three-body hardcore constraint which involves three-body inelastic losses [2], resulting in an extremely small lifetime of the atomic pairs. On the other hand, the formation of Feshbach molecules is rovibrationally unstable and can reduce to the lower levels very easily. At this point, it is believed that the interacting photons can form stable bound pairs which can provide a promising platform to explore various fundamental phenomena and further the scope for technological applications. Several successful attempts have been made to create bound states of photons under different conditions [6–8]. The primary thrust and interest in creating photonic bound states

rests not only on understanding the fundamental physics of nature but also on possible practical applications in waveguide QED experiments [9,10] and quantum simulation [11–14].

The realization of strong interaction between photons has been a topic of paramount interest in the past several decades. The interaction which is believed to exist in optical nonlinear media, however, does not possess enough nonlinearity to ensure strong interactions between photons. The field of quantum optics has paved the path in achieving strong nonlinearity in various exciting platforms such as the optical cavities and superconducting circuits [19–21]. Several path-breaking achievements have been made with cavity and circuit QED in recent years using the two-level artificial atoms (also known as qubits). In the many-body context, an array of such artificial atoms coupled with photons has been shown to exhibit interesting scenarios in the framework of the celebrated Jaynes-Cummings-Hubbard (JCH) model [22–29]. The quantum phase transition between the superfluid (SF) and the Mott insulator (MI) of polaritons (the quasiparticles composed of atomic excitations and cavity photons) is an important revelation of the competing photon-atom interactions inside the cavity and the photon hopping between different cavities [23,30]. Following this, many interesting quantum phenomena have been analyzed in the framework of the JCH model [31]. The phenomenal progress in understanding the many-body aspects of strongly correlated photons and the demand to fulfill the requirements necessary for quantum technologies have attracted enormous attention towards the study of the cavity and circuit QED [32]. Although primarily the atom-photon interactions in such systems are two-body and repulsive and attractive in nature [22], recent progress in manipulating three- and higher-level systems has provided opportunities to explore alternative scenarios in quantum simulations with multilevel systems [33–38].

Although the systems of atoms in optical cavities to understand the physics of light-matter interaction are well

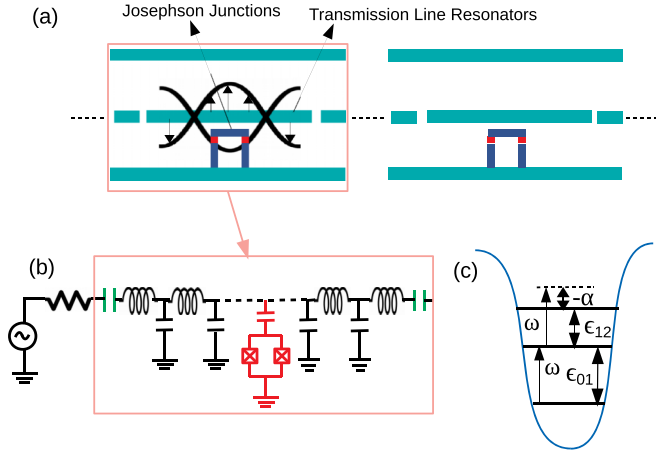


FIG. 1. (a) Schematic layout of an array of coupled cavity QED systems using transmons (not to scale) [15–18]. (b) Equivalent lumped circuit representation of a single transmon coupled to a single transmission line resonator by the coupling capacitors. Panel (c) shows the energy levels with only one driving frequency ω . We set $\omega = \epsilon_{01}$ ($\hbar = 1$) and $\alpha = \epsilon_{12} - \omega$.

established, the rapid developments in fabricating superconducting circuits have evolved as one of the most suited test beds for quantum simulations in recent years. The versatility of these systems arises from the flexibility to control the anharmonicity generated by the Josephson junctions which indirectly controls the interaction between the polaritons [39]. Motivated by all the recent developments we analyze the circuit QED of superconducting processors and propose a method to create photon pair propagation. Here we propose to use transmon [17,40,41] qubits truncated to the first three energy levels to create the bound photonic states.

The paper is organized as follows. In Sec. II, we discuss the results in one and two dimensions by introducing the Hamiltonian for this model. Section III contains the conclusion.

II. RESULTS

In this paper, we propose to use an array of transmission line resonators (TLRs) with capacitive coupling between two nearest neighbors and also each resonator coupled to a single transmon qubit truncated to the first three energy levels (known as qutrits). In Fig. 1 we present the case of a single transmon coupled to a single TLR via coupling capacitors and the TLRs are connected capacitively with one another. Here we consider the transmon mimicking an artificial three-level atomic system in a cascade (Ξ) configuration with unequal energy spacing's as depicted in Fig. 1(b). The energy difference between the levels $|0\rangle$ and $|1\rangle$ is denoted as ϵ_{01} , and the energy difference between levels $|1\rangle$ and $|2\rangle$ is denoted as ϵ_{12} . Here we consider that the transmons and the resonators are degenerate and therefore we set the cavity resonance frequency as $\omega = \epsilon_{01}$. We define $\alpha = \epsilon_{12} - \epsilon_{01}$ as the anharmonicity associated with the transmon. The cavity resonance frequency ω is chosen in such a way that it will drive the transmons between the levels $|0\rangle$ to $|1\rangle$ and $|1\rangle$ to $|2\rangle$, and all transitions to the higher excited levels are suppressed [42,43]. Employing the rotating-wave approximation [17], the many-body physics

of this system of coupled-cavity arrays can be analyzed in the context of the modified JCH model [18] given as follows:

$$\mathcal{H}_{\text{JCH}} = \sum_i \hbar[\alpha \hat{\sigma}_{2i}^\dagger \hat{\sigma}_{2i} + \beta_{12}(\hat{\sigma}_{2i}^\dagger \hat{a}_i + \text{H.c.}) + \beta_{01}(\hat{\sigma}_{1i}^\dagger \hat{a}_i + \text{H.c.})] - \hbar\kappa \sum_{(i,j)} (\hat{a}_i^\dagger \hat{a}_j + \text{H.c.}) \quad (1)$$

Here, a_i^\dagger (a_i) is the photonic creation (annihilation) operator, σ_{1i}^\dagger (σ_{2i}) is the atomic raising (lowering) operator which takes the atom from $|0\rangle_i$ to $|1\rangle_i$ ($|2\rangle_i$ to $|1\rangle_i$) levels, $n_i = n_i^p + \sigma_{1i}^\dagger \sigma_{1i} + \sigma_{2i}^\dagger \sigma_{2i}$ is the total polariton number at the i th cavity, and $n_i^p = a_i^\dagger a_i$ denotes the number operator of the photonic excitations. β_{01} (β_{12}) represents the atom-photon coupling strength between levels $|0\rangle$ and $|1\rangle$ ($|1\rangle$ and $|2\rangle$). The nearest-neighbor intercavity photon tunneling amplitude is denoted by κ . For our analysis, we define the polariton density as $\rho = N/L$, where $N = \sum_i n_i$ and L are the total number of polaritons and the total number of sites in the system, respectively.

As mentioned before in Sec. I, the two-level JCH model exhibits SF-MI phase transition as a function of the ratio κ/β_{01} . There exist the MI phases at integer polariton densities when the κ/β_{01} ratio is small and these phases are represented as MI(ρ). In the limit $\kappa \gg \beta_{01}$ the MI phases melt and a phase transition to the SF phase occurs due to the delocalization of photons. On the other hand, a recent mean-field study on a three-level atomic system with equally spaced levels in optical cavity arrays has predicted the complete suppression of the MI(1) lobe after a critical $\beta_{12}/\beta_{01} = \sqrt{2}$ [44]. In this limit, the MI(2) lobe is shown to overlap with the vacuum state and this signature is speculated to be of a pair-superfluid (PSF) phase of polaritons in analogy with the attractive Bose-Hubbard model. The key requirement to achieve this phenomenon is that the two transitions, $|0\rangle \rightarrow |1\rangle$ and $|1\rangle \rightarrow |2\rangle$, should be near resonantly driven by the same photon (including the polarization) which demands an equally spaced three-level Ξ system. However, we would like to stress that this condition is not satisfied by the natural atoms in optical cavities. Note that for the Λ and V systems the frequencies of two transitions can be the same but require different polarizations of the photons.

Interestingly, this condition can be easily satisfied in a transmon which plays the role of an artificial atom provided the higher energy levels except the first three are removed or truncated. The removal of the higher energy levels can be implemented by using strong anharmonicity to the system [17,45] as depicted in Fig. 1(b). Therefore, in our studies we consider a more realistic system of three-level artificial atoms by considering a transmon with unequal spacings which will circumvent the practical issues associated with an equally spaced Ξ system. Note that the anharmonicity naturally introduces the detuning for the $|1\rangle \rightarrow |2\rangle$ transition. To understand the effects of the strong correlations, we analyze the ground-state properties of the model given in Eq. (1) for one- and two-dimensional arrays of transmons using the density matrix renormalization group (DMRG) [46–48] method and the self-consistent cluster mean-field theory (CMFT) approach [49,50], respectively.

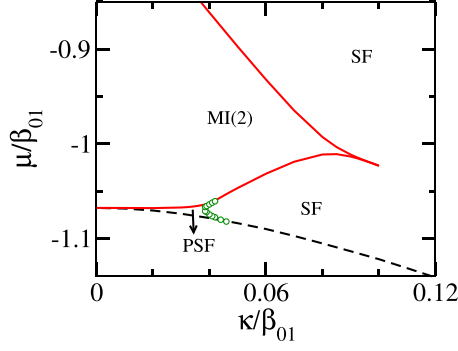


FIG. 2. Phase diagram of the JCH model using the DMRG method in one dimension for the anharmonicity $\alpha/\beta_{01} = -0.4$. In this figure the red solid curve demarcates the boundary of the MI(2) phase, the green circles show the PSF-SF phase boundary, and the black dashed curve is the vacuum state or the MI(0) phase. For the DMRG method in Fig. 2 all boundaries are calculated by extrapolating the chemical potential to thermodynamic limit using a maximum system size of $L = 80$ cavities.

A. Phase diagram in one dimension

In this part, we discuss the results in a one-dimensional circuit QED array with an experimentally realistic three-level Ξ system by considering $\beta_{12}/\beta_{01} = \sqrt{2}$ and finite anharmonicity $\alpha/\beta_{01} = -0.4$. Note that the ratio β_{12}/β_{01} is smaller than $\sqrt{2}$ due to the anharmonicity α . However, we have verified that the PSF phase exists for a wide range of the β_{12}/β_{01} ratio. It is to be noted that there is no particular reason behind this choice of $\alpha/\beta_{01} = -0.4$. To get a clear numerical picture, we keep the value of α/β_{01} close to the experimentally accessible regime [45]. By utilizing the DMRG method we compute the ground-state phase diagram in the plane of κ/β_{01} and μ/β_{01} as shown in Fig. 2, where μ is the chemical potential of the system. Note that the DMRG simulations are done in the canonical ensemble with a fixed polariton number and hence the Hamiltonian of Eq. (1) is explicitly independent of μ . It can be seen from the phase diagram that the MI(2) lobe (red solid curve) appears immediately after the vacuum state (black dashed line) by completely suppressing the MI(1) lobe which usually appears in the phase diagram of the JCH model of two-level systems [23]. Moreover, in this case, there is no overlap of the vacuum and the MI(2) lobe as opposed to the MFT results shown in Ref. [44] in the absence of any anharmonicity. Interestingly there exists a PSF phase of polaritons in the gapless region bounded by the green circles for small values of κ/β_{01} . Before going to the details of this PSF phase we first discuss the phase diagram in the following.

First of all, we trace out the phase transition from the gapped MI(2) phase to the SF phase of polaritons by looking at the energy gaps in the system. The signature of the gapped MI(2) phase is seen as the plateaus in the ρ vs μ/β_{01} plot at $\rho = 2$ as shown in Fig. 3(a), which is a signature of the gap in the system. The phase boundaries are obtained by computing the extrapolated values of the endpoints of the plateaus, which are the chemical potentials of the systems defined as $\mu^+ = E_{N+1} - E_N$ and $\mu^- = E_N - E_{N-1}$ in the thermodynamic limit for different values of κ/β_{01} . Here, E_N is the ground-state energy with N polaritons. Now we systematically analyze the

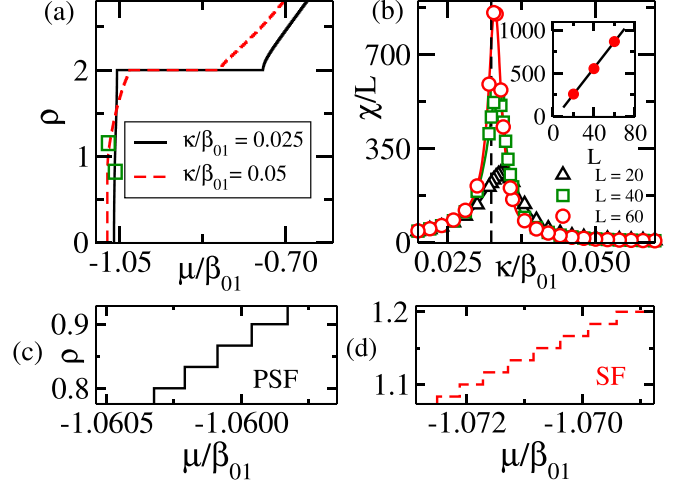


FIG. 3. (a) DMRG data shows the ρ vs μ/β_{01} plot for parameters $\kappa/\beta_{01} = 0.025$ and $\kappa/\beta_{01} = 0.05$ when $\alpha/\beta_{01} = -0.4$, indicating the SF and PSF regions for $L = 60$ sites. The regions marked by the green squares are enlarged in Figs. 3(c) and 3(d), which show the signatures of the PSF and the SF phases, respectively. (b) $\chi_{\text{FS}}(\tilde{\kappa})$ vs κ/β_{01} plots for different system sizes of $L = 20, 40$, and 60 to see the phase transition point. The inset shows that the peak heights diverge with system size, indicating the phase transition. The dashed vertical line corresponds to the critical point of the transition, determined by extrapolating the peak position to the thermodynamic limit.

signatures of the pair formation in the system. The immediate information can be obtained by analyzing the dependence of ρ with respect to μ/β_{01} for different values of κ/β_{01} . In Fig. 3(a) we plot ρ vs μ/β_{01} corresponding to two different values of $\kappa/\beta_{01} = 0.025$ (black solid line) and 0.05 (red dashed line) of the phase diagram in Fig. 2. Note that, when $\kappa/\beta_{01} = 0.05$, the value of ρ increases in steps of one particle, indicating the SF phase. However, for $\kappa/\beta_{01} = 0.025$, the value of ρ increases in steps corresponding to the change in polariton number $\Delta n = 2$ up to the MI(2) plateau from the bottom. This can be clearly seen from the zoomed-in regions plotted in Figs. 3(c) and 3(d) corresponding to the green boxes shown in Fig. 3(a). This indicates the quasiparticle excitations in terms of polariton pairs, which is a typical signature of the pair formation [4,51,52]. This phenomenon happens in the gapless region between the vacuum and the MI(2) phase in the regime of small κ/β_{01} and therefore can be called a PSF phase of polaritons. As a result, there exists a phase transition from the SF phase to the PSF phase as a function of κ/β_{01} , which is indicated by the green circles in Fig. 2. We compute the PSF-SF phase boundary from the ρ vs μ/β_{01} plot and complement it by looking at the divergence of the fidelity susceptibility [4,53] across the phase transition defined as

$$\chi_{\text{FS}}(\tilde{\kappa}) = \lim_{\tilde{\kappa} - \tilde{\kappa}' \rightarrow 0} \frac{-2 \ln |\langle \Psi_0(\tilde{\kappa}) | \Psi_0(\tilde{\kappa}') \rangle|}{(\tilde{\kappa} - \tilde{\kappa}')^2}, \quad (2)$$

at $\rho = 1.5$. Here $\tilde{\kappa} = \kappa/\beta_{01}$, $|\Psi_0\rangle$ is the ground-state wave function and $\tilde{\kappa}'$ is a small change in the rescaled hopping amplitude. From Fig. 3(b), we observe a diverging stable maximum with increasing system sizes which shows the PSF-SF phase transition point at $\kappa/\beta_{01} = 0.03237$.

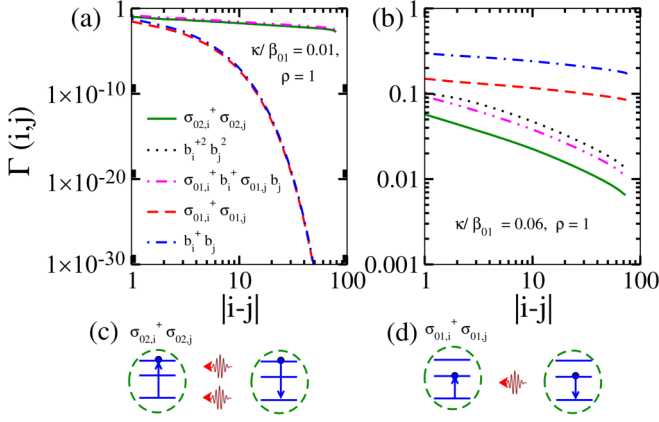


FIG. 4. The pair and single polariton correlation functions $\Gamma(i, j)$ with the distance $|i - j|$ for $\rho = 1$ with (a) $\kappa/\beta_{01} = 0.01$ and (b) $\kappa/\beta_{01} = 0.06$. Panels (c) and (d) show the two-photon and single-photon tunneling processes, respectively.

Although the ρ vs μ/β_{01} behavior allows us to identify the PSF phase of polaritons, it does not provide any insight about the underlying mechanism.

B. The PSF phase

Now we provide a detailed analysis of the physics of photon pair propagation and the PSF phase of polaritons. To understand the pairing phenomena we rely on the behavior of various single and pair correlation functions. In Fig. 4 we plot all the correlation functions with respect to the distance $|i - j|$ for a system of length $L = 80$ and $\kappa/\beta_{01} = 0.01$. Interestingly, it can be seen in Fig. 4(a) that the correlation function associated with the photon pairs which is defined as $\Gamma_{\text{photon-pair}}(i, j) = \langle b_i^\dagger b_j^\dagger \rangle$ (black dotted line) exhibits algebraic decay, whereas the single-photon correlation, i.e., $\Gamma_{\text{photon}}(i, j) = \langle b_i^\dagger b_j \rangle$ (blue dot-dashed line) decays exponentially. This is a clear indication of the existence of the long-range coherence of photon pairs in the system, and the single-particle motion is completely suppressed in the thermodynamic limit. At the same time, the atom-pair correlation defined as $\Gamma_{\text{atom-pair}}(i, j) = \langle \sigma_{02,i}^\dagger \sigma_{02,j} \rangle$ (green solid line) also remains finite, whereas the single-atom correlation $\Gamma_{\text{atom}}(i, j) = \langle \sigma_{01,i}^\dagger \sigma_{01,j} \rangle$ (red dashed line) vanishes exponentially across the array. This implies that a pair of photons gets spontaneously emitted from a cavity and gets absorbed by the nearest-neighbor cavity and excites the atom sitting there. This process continues resulting in the superfluid of photon pairs. Here $\sigma_{01,i}$ ($\sigma_{02,i}$) are the annihilation operators associated with the atomic excitations from the ground state to the first and second levels, respectively. On the other hand for large values of κ/β_{01} we have verified that the single-particle correlation functions dominate over the pair ones, justifying the SF phase as depicted in Fig. 4(b). The physical processes which may arise from single- and pair-photon propagations are depicted in Figs. 4(d) and 4(c), respectively. Interestingly, we also find that in the limit of two-photon propagation there exists finite correlation corresponding to the single photon and an atomic excitation that is $\Gamma_{\text{atom-photon}}(i, j) = \langle \sigma_{01,i}^\dagger b_i^\dagger \sigma_{01,j} b_j \rangle$. Hence in the present case, we can have three

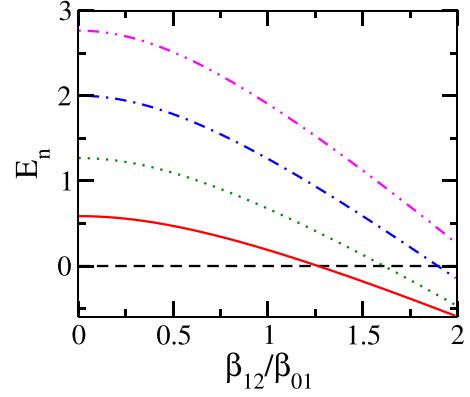


FIG. 5. The polariton energies E_n (bottom to top for $n = 1 \rightarrow 5$ at the origin) for $\mu/\beta_{01} = -1$ with respect to β_{12}/β_{01} for $\alpha/\beta_{01} = -0.4$.

different scenarios, such as (a) $|n_p = 2, n_a = 0\rangle$, (b) $|n_p = 1, n_a = 1\rangle$, and (c) $|n_p = 0, n_a = 2\rangle$, which can facilitate the photon pair propagation between the SQCs for small κ/β_{01} values. The physics behind such photonic pair creation or photon pair propagation can be understood by analyzing the energies associated with the system as done in Ref. [44]. In the SF regime where the single-photon processes take place, the artificial atom can go from $|n_a = 0\rangle$ to $|n_a = 1\rangle$, $|n_a = 1\rangle$ to $|n_a = 0\rangle$, $|n_a = 1\rangle$ to $|n_a = 2\rangle$, or $|n_a = 2\rangle$ to $|n_a = 1\rangle$ as shown in Fig. 4(d).

We show in Fig. 5 that for $\alpha/\beta_{01} = -0.4$, the cavity excitation energy corresponding to two-polariton becomes negative, whereas the energy corresponding to other higher polaritonic excitation remains positive well before $\beta_{12}/\beta_{01} = \sqrt{2}$. This promotes the formation of two polaritons in the transmons and indirectly the photon pair propagation. Therefore, the photon pair propagation and the associated polaritonic PSF phase in the three-level JCH model is not identical to the atomic PSF phase in the BH model due to the attractive interaction between bosons.

C. Phase diagram in two dimensions

After obtaining the signature of the photon pair propagation in the one-dimensional circuit QED setup, we analyzed the physics of the JCH model using the CMFT approach by going to two dimensions. Note that the CMFT approach works in the grand canonical ensemble, and hence we explicitly include the term associated with the chemical potential as $\mu \sum_i n_i$ in the JCH model given in Eq. (1). In this method, the entire system is divided into identical clusters of a limited number of sites which can be treated precisely and then the coupling between different clusters is treated in a mean-field way. The accuracy of this method improves by increasing the number of sites in the cluster. With this approximation the original Hamiltonian of Eq. (1) can be written as

$$\begin{aligned} \mathcal{H}_{\text{CMF}} &= \mathcal{H}_C + \mathcal{H}_{\text{MF}} \\ &= \mathcal{H}_C - \kappa \sum_{\langle i,j \rangle} [(a_i^\dagger + a_i)\psi_j - \psi_i^* \psi_j], \end{aligned} \quad (3)$$

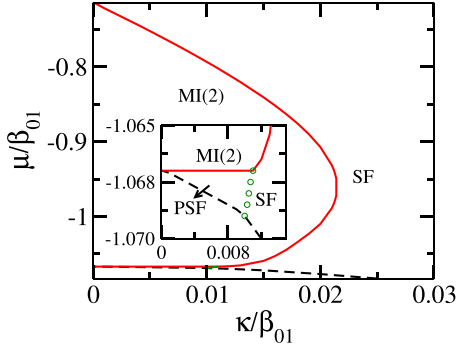


FIG. 6. Phase diagram of the JCH model using the CMFT method in two dimensions for the anharmonicity $\alpha/\beta_{01} = -0.4$. The red solid curve demarcates the boundary of the MI(2) phase, the green circles show the PSF-SF phase boundary, and the black dashed curve is the vacuum state or the MI(0) phase. In the inset, we show the enlarged PSF region.

where \mathcal{H}_C (\mathcal{H}_{MF}) is the cluster (mean-field) part of the Hamiltonian and $\psi_i = \langle a_i^\dagger \rangle = \langle a_i \rangle$ is the SF order parameter. The form of \mathcal{H}_C is same as Eq. (1) and is limited to the cluster only.

The self-consistent solution of the CMFT Hamiltonian yields the ground-state phase diagram in two dimensions as depicted in Fig. 6. It can be seen that the phase diagram in two dimensions is qualitatively similar to the one obtained for the one-dimensional case (Fig. 2). The phase diagram of Fig. 6 is obtained by looking at the behavior of the density $\rho = \frac{1}{L} \sum_i \hat{n}_i = \frac{1}{L} \sum_i (\hat{n}_i^p + \hat{n}_i^a)$ with respect to μ for different values of κ/β_{01} . In Fig. 7(a), we plot the values of ρ vs μ/β_{01} along with the cuts through the CMFT phase diagram of Fig. 6 at $\kappa/\beta_{01} = 0.01$ and $\kappa/\beta_{01} = 0.02$ which passes through different phases. The discrete jumps in the ρ - μ/β_{01} plot (black circles) in steps of two particles are an indication of the PSF phase as discussed in Sec. II B and the plateaus at $\rho = 2$ correspond to the MI(2) phase. We also plot the correlation functions for a single photon, a pair of photons, a single atom, and a pair of atoms, as shown in Fig. 7(b). As the cluster is of four sites only, the correlations are computed between the nearest neighbors and by averaging them over the entire cluster. This clearly shows the dominant pair correlation

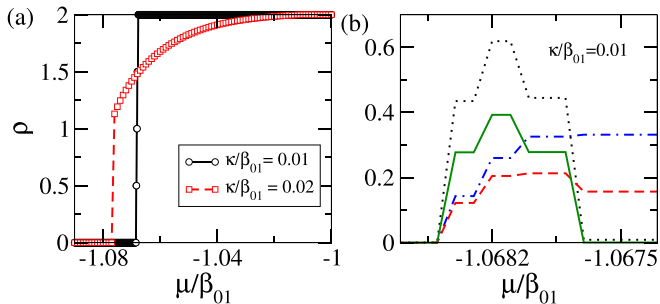


FIG. 7. (a) ρ - μ/β_{01} plot at $\kappa/\beta_{01} = 0.01$ and 0.02 of Fig. 6. (b) Different correlation functions such as $\Gamma_{\text{atom-pair}}(i, j)$ (green solid line), $\Gamma_{\text{photon}}(i, j)$ (blue dot-dashed line), $\Gamma_{\text{photon-pair}}(i, j)$ (black dotted line), and $\Gamma_{\text{atom}}(i, j)$ (red dashed line) are plotted for $\kappa/\beta_{01} = 0.01$ (see text).

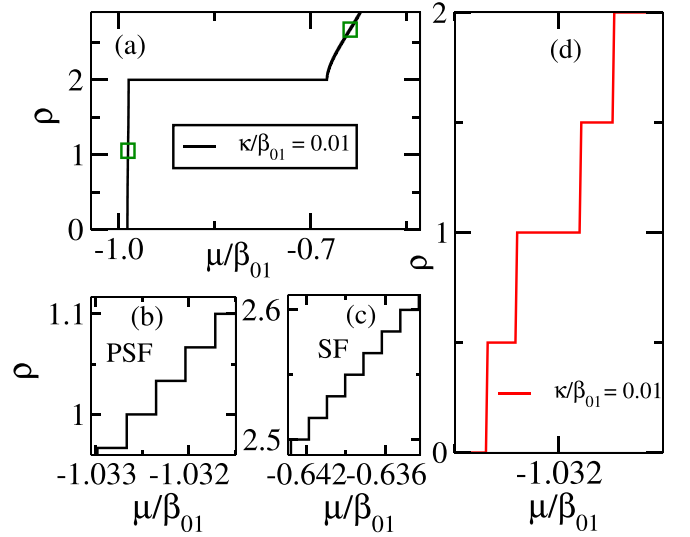


FIG. 8. (a) DMRG data shows the ρ vs μ/β_{01} plot (black solid line) for parameters $\kappa/\beta_{01} = 0.01$ when $\alpha/\beta_{01} = -0.4$, indicating the PSF and SF regions for $L = 60$ sites in one dimension. The regions marked by the green squares are enlarged in Figs. 8(b) and 8(c), which show the signatures of the PSF and the SF phases, respectively. (d) CMFT data for the ρ vs μ/β_{01} plot (red solid line) for $\kappa/\beta_{01} = 0.01$ and $\alpha/\beta_{01} = -0.4$, indicating the PSF phase for four sites in two dimensions.

functions as compared to the single-particle ones (see figure caption for details).

III. CONCLUSIONS

In this work, we propose a scheme for spontaneous photon pair creation and propagation in an array of coupled transmons. Considering the three-level artificial atoms of the Ξ type instead of the usual two-level qubit systems, we analyze the corresponding Jaynes-Cummings-Hubbard model in one- and two-dimensional arrays using the DMRG and the CMFT approach to establish the emergent photon pair propagation in the system. We show that, for the suitable ratio of the coupling strengths between different levels, the single-photon tunneling is suppressed, and photons tend to move in pairs. This two-photon propagation leads to the formation of the polaritonic pair-superfluid phase, located between the vacuum and the MI(2) phases of the polaritonic phase diagram. This finding is obtained by considering a more realistic setup of the transmons of a three-level atom with unequal level spacings that are experimentally more feasible than the optical cavity-atom arrangements. We would like to note that, in this case, there exists no overlap between the vacuum state and the MI(2) phase or the first-order-type phase transition as predicted earlier using the MFT approach [44]. This inconsistency can be attributed to the artifact of the simple mean-field theory approach in which it is difficult to capture all the relevant physics arising due to the off-site correlations as rightly mentioned in Ref. [44].

This analysis provides a promising platform to observe the pairing phenomena of bosons in general as compared to its atomic and molecular counterparts. Moreover, this

finding in the three-level system can be made useful for quantum communications [11–14,54–57] in the future as a bound state of photons is believed to carry more information than the individual photon. This work can shed light on the controlled creation and manipulation of boson pairs and can be extended to create higher-order photonic bound states (trimers, etc.) in an array of multilevel artificial atoms.

ACKNOWLEDGMENTS

T.M. acknowledges DST-SERB for the early career grant through Project No. ECR/2017/001069. K.P. acknowledges funding from SERB of Grant No. ECR/2017/000781. Part of the computational simulations were carried out using the Param-Ishan HPC facility at the Indian Institute of Technology Guwahati, India.

APPENDIX: PSF PHASE IN THE EXPERIMENTALLY REALIZABLE REGIME

In the experimentally realizable regime, the value of β_{12}/β_{01} must be less than $\sqrt{2}$ due to the finite anharmonicity of the transmon. Here we consider the case where $\beta_{12}/\beta_{01} = 1.35$, $\kappa/\beta_{01} = 0.01$, and $\alpha/\beta_{01} = -0.4$ and obtain the signature of PSF phase for both one- and two-dimensional systems using the DMRG and the CMFT methods, respectively, as shown in Fig. 8. In Fig. 8(a), we plot the ρ vs μ/β_{01} data obtained using the DMRG method. In the PSF region, the discrete jumps in density ρ correspond to the change in polariton number $\Delta n = 2$, whereas in the SF region the polariton number changes in steps of $\Delta n = 1$, as indicated in the zoomed-in regions plotted in Figs. 8(b) and 8(c), respectively. In Fig. 8(d) we plot the ρ vs μ/β_{01} data obtained using the CMFT method for $\kappa/\beta_{01} = 0.01$, showing the discrete jumps in steps of two particles, which indicates the PSF phase of polaritons.

-
- [1] N. W. Ashcroft and N. D. Mermin, *Solid State Physics* (Saunders College, Philadelphia, 1976).
- [2] A. J. Daley, J. M. Taylor, S. Diehl, M. Baranov, and P. Zoller, *Phys. Rev. Lett.* **102**, 040402 (2009).
- [3] J. P. Covey, S. A. Moses, M. Gärttner, A. Safavi-Naini, M. T. Miecnikowski, Z. Fu, J. Schachenmayer, P. S. Julienne, A. M. Rey, D. S. Jin *et al.*, *Nat. Commun.* **7**, 11279 (2016).
- [4] M. Singh, S. Greschner, and T. Mishra, *Phys. Rev. A* **98**, 023615 (2018).
- [5] D. van Oosten, P. van der Straten, and H. T. C. Stoof, *Phys. Rev. A* **63**, 053601 (2001).
- [6] O. Firstenberg, T. Peyronel, Q.-Y. Liang, A. V. Gorshkov, M. D. Lukin, and V. Vuletic, *Nature (London)* **502**, 71 (2013).
- [7] Q.-Y. Liang, A. V. Venkatramani, S. H. Cantu, T. L. Nicholson, M. J. Gullans, A. V. Gorshkov, J. D. Thompson, C. Chin, M. D. Lukin, and V. Vuletic, *Science* **359**, 783 (2018).
- [8] N. Rivera, G. Rosolen, J. D. Joannopoulos, I. Kaminer, and M. Soljacic, *Proc. Natl. Acad. Sci. USA* **114**, 13607 (2017).
- [9] J. C. F. Matthews, A. Politi, A. Stefanov, and J. L. O'Brien, *Nat. Photonics* **3**, 346 (2009).
- [10] N. Matsuda and H. Takesue, *Nanophotonics* **5**, 440 (2016).
- [11] E. Pomarico, B. Sanguinetti, N. Gisin, R. Thew, H. Zbinden, G. Schreiber, A. Thomas, and W. Sohler, *New J. Phys.* **11**, 113042 (2009).
- [12] C. Clausen, C. Bussi eres, A. Tiranov, H. Herrmann, C. Silberhorn, W. Sohler, M. Afzelius, and N. Gisin, *New J. Phys.* **16**, 093058 (2014).
- [13] P.-J. Tsai and Y.-C. Chen, *Quantum Sci. Technol.* **3**, 034005 (2018).
- [14] A. Veps al inen, S. Danilin, and G. S. Paraoanu, *Sci. Adv.* **5**, eaau5999 (2019).
- [15] A. Blais, R.-S. Huang, A. Wallraff, S. M. Girvin, and R. J. Schoelkopf, *Phys. Rev. A* **69**, 062320 (2004).
- [16] A. Blais, J. Gambetta, A. Wallraff, D. I. Schuster, S. M. Girvin, M. H. Devoret, and R. J. Schoelkopf, *Phys. Rev. A* **75**, 032329 (2007).
- [17] J. Koch, T. M. Yu, J. Gambetta, A. A. Houck, D. I. Schuster, J. Majer, A. Blais, M. H. Devoret, S. M. Girvin, and R. J. Schoelkopf, *Phys. Rev. A* **76**, 042319 (2007).
- [18] A. A. Houck, H. E. T ureci, and J. Koch, *Nat. Phys.* **8**, 292 (2012).
- [19] D. E. Chang, V. Vuletic, and M. D. Lukin, *Nat. Photonics* **8**, 685 (2014).
- [20] M. J. Hartmann, *J. Opt.* **18**, 104005 (2016).
- [21] A. Wallraff, D. I. Schuster, A. Blais, L. Frunzio, R.-S. Huang, J. Majer, S. Kumar, S. M. Girvin, and R. J. Schoelkopf, *Nature (London)* **431**, 162 (2004).
- [22] M. J. Hartmann, F. G. Brandao, and M. B. Plenio, *Nat. Phys.* **2**, 849 (2006).
- [23] A. D. Greentree, C. Tahan, J. H. Cole, and L. C. Hollenberg, *Nat. Phys.* **2**, 856 (2006).
- [24] M. I. Makin, J. H. Cole, C. Tahan, L. C. L. Hollenberg, and A. D. Greentree, *Phys. Rev. A* **77**, 053819 (2008).
- [25] A. Mering, M. Fleischhauer, P. A. Ivanov, and K. Singer, *Phys. Rev. A* **80**, 053821 (2009).
- [26] S. Schmidt and G. Blatter, *Phys. Rev. Lett.* **103**, 086403 (2009).
- [27] J. Koch and K. Le Hur, *Phys. Rev. A* **80**, 023811 (2009).
- [28] M. Hohenadler, M. Aichhorn, L. Pollet, and S. Schmidt, *Phys. Rev. A* **85**, 013810 (2012).
- [29] K. Toyoda, Y. Matsuno, A. Noguchi, S. Haze, and S. Urabe, *Phys. Rev. Lett.* **111**, 160501 (2013).
- [30] L.-L. Zheng, K.-M. Li, X.-Y. L u, and Y. Wu, *Phys. Rev. A* **96**, 053809 (2017).
- [31] J. Zhang and Y. Jiang, *Laser Phys.* **27**, 035203 (2017).
- [32] C. Noh and D. G. Angelakis, *Rep. Prog. Phys.* **80**, 016401 (2016).
- [33] M. Alexanian, *Phys. Rev. A* **83**, 023814 (2011).
- [34] I. Pietik ainen, S. Danilin, K. S. Kumar, A. Veps al inen, D. S. Golubev, J. Tuorila, and G. S. Paraoanu, *Phys. Rev. B* **96**, 020501(R) (2017).
- [35] I. Pietik ainen, S. Danilin, K. S. Kumar, J. Tuorila, and G. S. Paraoanu, *J. Low Temp. Phys.* **191**, 354 (2018).
- [36] Y.-H. Luo, H.-S. Zhong, M. Erhard, X.-L. Wang, L.-C. Peng, M. Krenn, X. Jiang, L. Li, N.-L. Liu, C.-Y. Lu *et al.*, *Phys. Rev. Lett.* **123**, 070505 (2019).
- [37] X.-M. Hu, C. Zhang, B.-H. Liu, Y.-F. Huang, C.-F. Li, and G.-C. Guo, *arXiv:1904.12249*.

- [38] I. Pietikäinen, J. Tuorila, D. S. Golubev, and G. S. Paraoanu, *Phys. Rev. A* **99**, 063828 (2019).
- [39] S. Schmidt and J. Koch, *Ann. Phys.* **525**, 395 (2013).
- [40] J. A. Schreier, A. A. Houck, J. Koch, D. I. Schuster, B. R. Johnson, J. M. Chow, J. M. Gambetta, J. Majer, L. Frunzio, M. H. Devoret, S. M. Girvin, and R. J. Schoelkopf, *Phys. Rev. B* **77**, 180502(R) (2008).
- [41] Y. Chen, C. Neill, P. Roushan, N. Leung, M. Fang, R. Barends, J. Kelly, B. Campbell, Z. Chen, B. Chiaro *et al.*, *Phys. Rev. Lett.* **113**, 220502 (2014).
- [42] M. Baur, S. Filipp, R. Bianchetti, J. M. Fink, M. Göppl, L. Steffen, P. J. Leek, A. Blais, and A. Wallraff, *Phys. Rev. Lett.* **102**, 243602 (2009).
- [43] R. Bianchetti, S. Filipp, M. Baur, J. M. Fink, C. Lang, L. Steffen, M. Boissonneault, A. Blais, and A. Wallraff, *Phys. Rev. Lett.* **105**, 223601 (2010).
- [44] S. B. Prasad and A. M. Martin, *Sci. Rep.* **8**, 16253 (2018).
- [45] J. M. Martinis, S. Nam, J. Aumentado, and C. Urbina, *Phys. Rev. Lett.* **89**, 117901 (2002).
- [46] S. R. White, *Phys. Rev. Lett.* **69**, 2863 (1992).
- [47] U. Schollwöck, *Rev. Mod. Phys.* **77**, 259 (2005).
- [48] U. Schollwöck, *Ann. Phys.* **326**, 96 (2011).
- [49] T. McIntosh, P. Pisarski, R. J. Gooding, and E. Zaremba, *Phys. Rev. A* **86**, 013623 (2012).
- [50] M. Singh, S. Mondal, B. K. Sahoo, and T. Mishra, *Phys. Rev. A* **96**, 053604 (2017).
- [51] T. Mishra, S. Greschner, and L. Santos, *Phys. Rev. A* **91**, 043614 (2015).
- [52] S. Mondal, S. Greschner, and T. Mishra, *Phys. Rev. A* **100**, 013627 (2019).
- [53] S.-J. Gu, *Int. J. Mod. Phys. B* **24**, 4371 (2010).
- [54] C. E. Kuklewicz, F. N. C. Wong, and J. H. Shapiro, *Phys. Rev. Lett.* **97**, 223601 (2006).
- [55] X.-H. Bao, Y. Qian, J. Yang, H. Zhang, Z.-B. Chen, T. Yang, and J.-W. Pan, *Phys. Rev. Lett.* **101**, 190501 (2008).
- [56] F. Wolfgramm, X. Xing, A. Cerè, A. Predojević, A. M. Steinberg, and M. W. Mitchell, *Opt. Express* **16**, 18145 (2008).
- [57] A. Haase, N. Piro, J. Eschner, and M. W. Mitchell, *Optics Lett.* **34**, 55 (2009).